International Journal of Bioprinting

RESEARCH ARTICLE

In situ defect detection and feedback control with three-dimensional extrusion-based bioprinter-associated optical coherence tomography

Supplementary File

In the previous study, the simplified iterative closest point (ICP) algorithm based on a point cloud has been proposed to achieve large-field, full-depth imaging. The lateral field expansion process is shown in Supplementary Figure S1, including feature point extraction, point cloud generation, overlapped area extraction, point cloud registration based on a simplified ICP and rigid transformation of the point cloud. The input datasets I_n and I_{n-1} were two series of 3D P-OCT intensity images acquired from the adjacent field after preprocessing. The feature points were extracted after surface profile identification based on the maximum intensity value of each A-line (Figure S1(b)). Subsequently, the feature point clouds of two adjacent 3D P-OCT datasets were generated (see PT_{n-1} and PT_{n-1} in Figure S1(c)) based on the point cloud generation algorithm described in Table S1.

Furthermore, based on the prior acquisition information of the OCT probe displacement, the points located in the overlapping area between PT_n and PT_{n-1} were extracted (see the red and green point clouds in Figure S1(d)). When ignoring the mechanical errors, there was a 10% (equivalent to a 1mm size) overlap between adjacent datasets. To ensure that the source point cloud contained the target point cloud, an extra 2% of points were extracted from PT_{n-1} as the source point cloud PT'_{n-1} and there were 2% of points not extracted from PT_n as the target point cloud PT'_{n-1}. Before the simplified ICP iterations, the point cloud was roughly registered according to the displacement of the OCT probe, to prevent the ICP algorithm from falling into the local minimum solution (see the rough registration in Figure S1(e)). Subsequently, simplified ICP iterations were applied for the iterative registration of two point clouds (see the precise registration in Figure S1(e)). In this study, the maximum iteration number was set to 1000 and the convergence distance was set to 0.001 Euclidean distance. In addition, the rigid transformation matrix $T_{n,n-1}$ can be generated for the original adjacent OCT datasets (Figure S1(f)). The first three values in the fourth column of the matrix refer to the offsets of the three directions (X-Y-Z). When there are multiple 3D P-OCT datasets in the same layer, the above steps can be performed successively to generate the large-field imaging result I^l for the current l_t layer, which can be used for defect detection, location and feedback.

The longitudinal depth expansion process was performed after the lateral field expansion, as shown in Figure 2(g-j), including feature point extraction, point cloud generation, point extraction for the current layer, point cloud registration based on simplified ICP, and rigid transformation of the point cloud. Briefly, the input datasets were the large-field imaging results I^l for the l_{th} layer and I^{l-1} for the $l\text{-}1_{th}$ layer. The surface point clouds were generated PT^l and PT^{l-1} with the previous algorithm in the lateral field expansion. Considering the interleaved printing path of different layers, OCT imaging results might contain several layers of structural information. For longitudinal registration , the point clouds of the same layer (the $l\text{-}1_{th}$ layer) should be extracted from the large-field imaging results, I^l and I^{l-1}. As shown in Figure S1(h), the method of frequency statistics of the z coordinates was used to extract points located only in the $l\text{-}1_{th}$ layer from I^l and I^{l-1}. Specifically, the frequency statistics of the z-coordinates of point clouds PT^l and PT^{l-1} were shown in Figure S1(h), and there are several peaks corresponding to several different layers. For PT^{l-1}, the first peak represented surface points of the $l\text{-}1_{th}$ layer, which can extracted and denoted as PT'^{l-1}; for PT^l, the second peak represented surface points of the $l\text{-}1_{th}$ layer, which can extracted and denoted as PT''^{l-1}. Because both point clouds PT'^{l-1} and PT''^{l-1} were the surface points from the $l\text{-}1_{th}$ layer, the displacement information of OCT probe can be used as the rough registration basis to avoid overfitting (see the rough registration in Figure S1(i)). Simplified ICP iterations were then applied for precise registration of the two point clouds (see the precise registration in Figure S1(i)). Subsequently, the rigid transformation matrix can be generated for the longitudinal mosaics (Figure S1(j)).

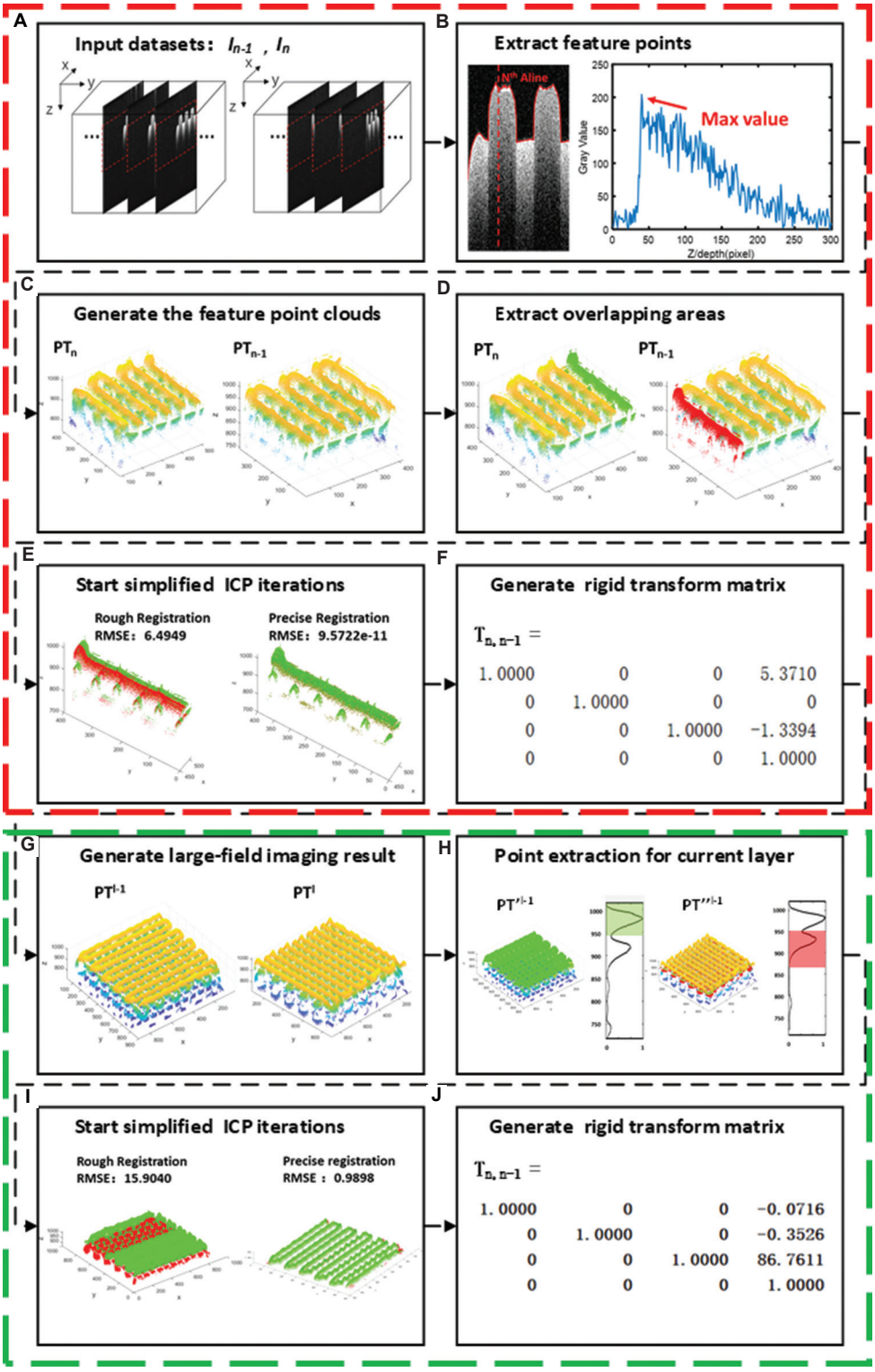

Supplementary Figure S1. The flow chart for large-field (A-F) and full-depth (G-J) imaging strategy in 3D P-OCT.

Table S1. Generation pseudocode of the feature point cloud.

1 *Algorithm*1 : *generatePointCloud*

```
function GETPOINTCLOUD(volumeData)
    xRecord = []; yRecord = []; zRecord = [];
    for i = 1 → size(volumeData, 3) do
        img = volumeData(:, :, i);
        T = graythresh(img);
        imgBw = rgb2gray(img, T);
        imgSurf = peak2surface(imgBw);
        [z, x] = find(imgSurf == 1);
        y = ones(size(z)) ∗ (size(volumeData, 3) + 1 − i);
        xRecord = [xRecord; x]; yRecord = [yRecord; y]; zRecord = [zRecord; z];
    end for
    materialPC = [xRecord, yRecord, zRecord]′;
    return materialPc;
end function
```